Am J Transl Res 2023;15(3):1730-1743
www.ajtr.org /ISSN:1943-8141/AJTR0146631

Original Article

Construction of immune cell infiltration score model to assess prognostic ability of tumor immune environment in lung adenocarcinoma

Jiahui Tian[1,2*], Chunyan Fu[1,2*], Qian Peng[2], Jialu Yang[1], Xiaoxiao Fan[1], Xuan Zeng[2], Weiguo Qing[1#], Yi Wu[1,2#]

[1]Department of Laboratory, The First Affiliated Hospital of Hunan Normal University, Changsha 410005, Hunan, China; [2]Department of Medicine, Hunan Normal University, Changsha 410005, Hunan, China. [*]Equal contributors. [#]Equal contributors.

Received September 21, 2022; Accepted March 4, 2023; Epub March 15, 2023; Published March 30, 2023

Abstract: Objectives: The immune cell infiltration (ICI) in the tumor microenvironment (TME) can provide a reference for prognosis after immunotherapy. We aim to establish an ICI scoring model and evaluate its predictive ability for the immunotherapy efficacy and the prognosis in lung adenocarcinoma (LUAD) patients. Methods: We developed and analyzed the landscape of infiltrative immune cells based on the CIBERSORT and ESTIMATE algorithms. Then, three clusters of LUAD patients were discerned from TCGA-LUAD and GSE11969 data. Furthermore, two gene clusters were classified based on the PCA. Results: LUAD patients with better prognoses tend to have higher immune checkpoint expression and immune/stromal scores. There is a correlation between TMB and ICI, and their relationship deserves further exploration. Moreover, the early-stage and male patients with high ICI scores have more prolonged survival. Conclusions: The feasibility of the ICI score model in evaluating prognosis after immune checkpoint therapy for LUAD patients was verified, specifically reflected in the screening of sensitive immune checkpoints as a treatment reference. The scoring system can accurately predict the overall survival of LUAD patients, which has clinical value to monitor disease and evaluate prognosis.

Keywords: Lung adenocarcinoma, immune cell infiltration, tumor microenvironment, immunotherapy, prognosis evaluation

Introduction

Lung adenocarcinoma (LUAD), accounting for 50% of non-small cell lung cancer (NSCLC), has high heterogeneity and mortality among all cancers [1, 2]. Despite early diagnosis and treatment, the recurrence rate in LUAD patients is as high as 90% because of limited technology, and the 5-year survival rate is less than 15% [1, 3, 4].

The tumor microenvironment (TME), a complex environment in the tumor, consists of immune cells, stromal cells, extracellular matrix, and other cellular and non-cellular components, and mediates tumor occurrence, development, invasion, and immunosuppression [5-8]. Immunotherapy has emerged as a new approach for cancer treatment, but many patients with lung cancer demonstrate poor response to immunotherapy due to the limitation of TME-induced immunosuppression [9-11]. Therefore, overcoming immunosuppression is key to improving immunotherapy.

A poor TME regulates immune cells to enhance anti-tumor immunity, and targeting TME is expected to overcome immunosuppression and become a promising strategy for cancer immunotherapy [12-14]. Targeted tumor-associated macrophages (TAM) have been reported to overcome immune resistance induced by suppressive myeloid cells and to enhance tumor response to immune checkpoint inhibitors [15, 16]. Zeng et al. reported that immune-cell infiltration (ICI) in TME supported cancer metastasis and has been widely researched for its therapeutic promise as novel targets [17-19]. In the future, targeting ICI based on TME will inevitably become a strategy to alleviate immunosuppres-

sion. But few studies have specified the value of ICI for cancer immunotherapy and survival evaluation.

TMB is reported as a new signature for immune-checkpoint inhibitors to predict the efficacy of immunotherapy, and the mutation status of key genes may be associated with the distribution of immune infiltrating cells [20, 21]. Many studies proved that there might be a synergistic effect of ICI and TMB, and the relationship between TMB and immune infiltration depends on the cancer type [22, 23]. Therefore, exploring the correlation between ICI and TMB has important clinical significance for LUAD patients.

In this study, we established and analyzed the spectrum of ICI to quantify tumor-infiltrating immune cells. Subsequently, patients were assigned to three ICI clusters according to their ICI level. In addition, two gene clusters were discerned from differentially expressed genes. Last, the ICI scoring system was established to provide forward-looking evidence for the application of targeted TME in immunotherapy and predict the prognosis of LUAD patients.

Materials and methods

Source of lung adenocarcinoma data

The RNA-seq data, clinical data, and mutation data were procured from The Cancer Genome Atlas (TCGA). The transcriptome profiles and clinical data were obtained from Gene Expression Omnibus (GEO: GSE11969). To ensure the accuracy of expression profiles from TCGA-LUAD (FPKM values) in subsequent analysis, they was transformed into transcripts per kilobase million (TPM) values.

The analysis of infiltrative immune cells in TME

The TCGA and GEO data were consolidated for follow-up analysis, quantitative analysis of gene expression levels in 22 tumor-infiltrating immune cells was conducted by CIBERSORT algorithm, and the sum of immune and stromal scores was calculated through *ESTIMATE* R package. *Corrplot* R package was applied to analyze the correlation of TIICs. Data were repeatedly analyzed 1000X by ConsensusClusterPlus R package to identify cluster classification. We carried out the survival analysis based on merged data from TCGA-LUAD and GSE11969, and incomplete data were eliminated.

Identification of differentially expressed genes (DEGs)

The patients were assigned into three groups according to ICI levels and the DEGs were identified using limma R package. Fundamental criteria deserving consideration included $P<0.05$ and $|logFC| \geq 1$.

Computation of immune cell infiltration (ICI) score and analysis of mutation data

We performed unsupervised clustering to group LUAD patients per DEGs, in which positively related DEGs were defined as ICI gene signatures A and negatively related DEGs as ICI gene signatures B. The Boruta algorithm was applied for low-dimensional settings including ICI gene signatures A and B to screen out the optimal data sets [24], and principal component 1 (PC1) was procured as a signature score utilizing the principal-component analysis (PCA) [25]. The ICI score for each data can be computed through the following formula:

ICI Score = $\Sigma PC1_A$-$\Sigma PC1_B$ [26].

The TCGA-LUAD mutation cohort was collected from the TCGA dataset. After calculating the sum of nonsynonymous mutations, somatic mutations in driving genes were analyzed, using the maftools R package.

Statistical analysis

A comparison between the two groups was verified through the Wilcoxon test, while the comparison between the above two groups was implemented by the Kruskal-Wallis test [27, 28]. Survival curves were drawn by Kaplan-Meier plotter and survival differences were obtained by log-rank test. An unsupervised clustering was performed through Euclidean and Ward's linkage analysis. The high and low ICI subgroups were discerned based on the surv-cutpoint function. The chi-square test was conducted to compare the difference of somatic mutation frequency between different groups. The correlation coefficient was evaluated using the Spearman analysis. A difference was called significant if two-tailed $P<0.05$.

Results

The profile of immune cell infiltration in TME

The 564 samples from TCGA-LUAD and 149 samples from GSE11969 with RNA-seq data were processed. The workflow of the research is shown in **Figure 1**.

The sum of ICI scores was calculated via CIBERSORT algorithm and *ESTIMATE* R package. The ConsensusClusterPlus R packet was imposed to divide the patients into different clusters that were the optimal number of clusters, based on k=3, three clusters (ICI cluster A, B, and C) were discerned (Supplementary Figure 1). Differentially expressed genes between cluster A, B and C are shown in Supplementary Tables 1, 2, 3. There were no significant differences in overall survival seen in three clusters (**Figure 2A**, P=0.232). To further examine the expression difference of immune cells in the three clusters, a heatmap analysis was further carried out and the landscape was visualized (**Figure 2B**, **2C**). Furthermore, the correlation coefficient heatmap proved insight to uncover the intrinsic relativity of tumor-infiltrating immune cells in the TME (**Figure 2D**). Next, three important immune checkpoint molecules, PDCD1, LAG3, and CTLA4, and their expression were evaluated. The expression of the three was higher in cluster C than cluster A, but a statistical difference did not exist between cluster B and C (**Figure 2E-G**).

Discrimination of immune gene subtypes

Gene clusters were classified into two groups from differentially expressed genes: gene clusters A, and B (Supplementary Figure 2), based on the analysis of unsupervised clustering (**Figure 3A**). A significant difference in overall survival existed between gene clusters A and B (**Figure 3B**, P=0.016). The expression of 22 tumor-infiltrating immune cells among different gene clusters was compared, and we found that gene cluster A had a higher proportion of CD4 memory resting T cells, NK activated cells, M2 macrophages, dendritic cells, mast resting cells, neutrophil, and monocytes. Gene cluster B performed better in terms of immune filter scores, B naive cells, plasma cells, and CD4 memory activated T cells (**Figure 3C**). The expression of PDCD1, CTLA4, CD28, and LAG3 in gene cluster B reached the highest level. The results were also concordant with the higher immune and stromal filter scores in gene cluster B. These results suggested that patients in gene cluster B may reach favorable outcomes with immune checkpoint inhibitor therapy, for instance, PDCD1 and CTLA4 (**Figure 3D-G**).

Establishment and analysis of an ICI score model

First, ICI score was determined per PCA [29, 30], and then the best cutoff value was acquired to dichotomize patients into high and low ICI score subgroups. The correlation between gene cluster, ICI score, and patient fustat was visualized by alluvial diagram (**Figure 4A**). Next, we examined immune checkpoint/chemotactic-related genes to evaluate the immune activity in two subgroups, and five genes were recognized as inhibitory immune checkpoint genes (HAVCR2, CTLA4, CD160, and PDCD1). Four genes were recognized as the activated immune checkpoint genes (CD28, CD226, ICOS, and TNFRSF9); seven genes were recognized as the chemotactic-related immune genes (TNF, TBX2, CCL2, CX3CL1, CXCL2, CXCL3, and CCL19). We finally found that all genes except TNFRSF9 and PDCD1 showed higher expression levels in the high ICI score group compared to the low ICI score group (**Figure 4B**). Subsequently, we conducted gene ontology (GO) enrichment analysis. ICI gene signature A was enriched in gland development, external side of plasma membrane, transcription regulator complex, and signaling receptor activator activity (**Figure 4C**). ICI gene signature B was strongly related to many functions, including myeloid leukocyte migration, cell chemotaxis, phagocytosis collagen trimer, and endocytosis (**Figure 4D**).

Moreover, the GSEA results revealed that vascular smooth muscle contraction, complement and coagulation cascades, vasopressin regulated water reabsorption, calcium signaling pathway, and the Fc epsilon RI signaling pathway were significantly enriched in the high ICI score group. Spliceosome, proteasome, protein export, DNA replication, and mismatch repair were enriched in the low ICI score group (**Figure 4E**, P<0.05). In addition, a significant survival difference was observed in between high and low ICI score groups, and high ICI score correlated with better survival in TCGA-LUAD (P=0.006), GEO (P=0.027), and the com-

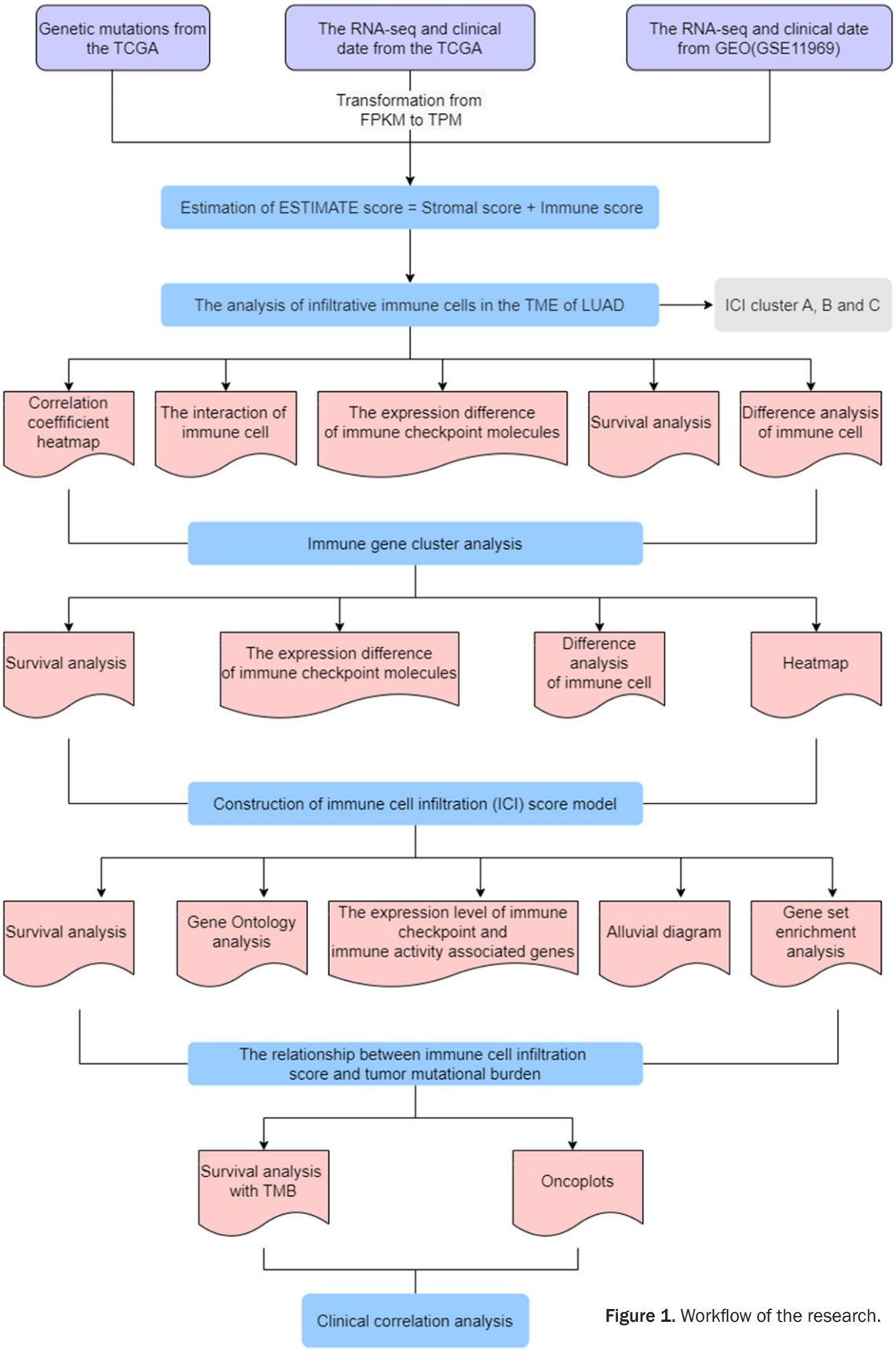

Figure 1. Workflow of the research.

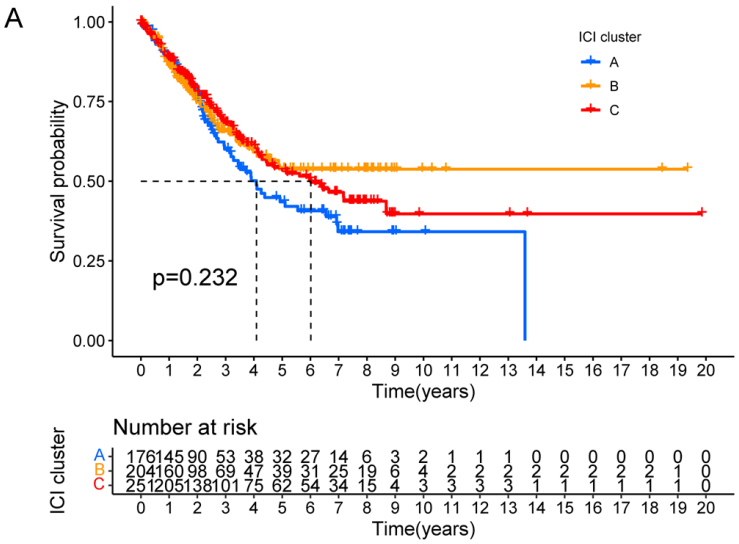
A
ICI cluster
A
B
C
Survival probability
1.00
0.75
0.50
0.25
0.00
p=0.232
0 1 2 3 4 5 6 7 8 9 10 11 12 13 14 15 16 17 18 19 20
Time(years)
Number at risk
ICI cluster
A 176 145 90 53 38 32 27 14 6 3 2 1 1 1 0 0 0 0 0 0 0
B 204 160 98 69 47 39 31 25 19 6 4 2 2 2 2 2 2 2 1 0
C 251 205 138 101 75 62 54 34 15 4 3 3 3 3 1 1 1 1 1 1 0
0 1 2 3 4 5 6 7 8 9 10 11 12 13 14 15 16 17 18 19 20
Time(years)

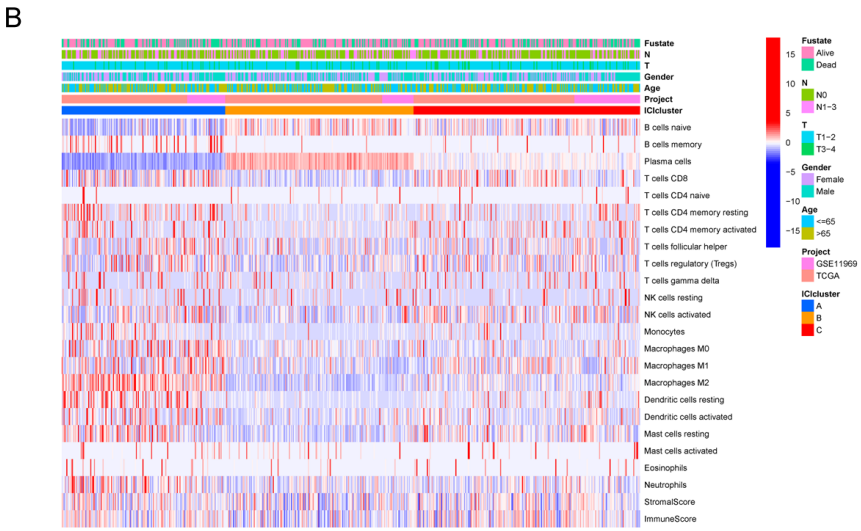
B
Fustate
N
T
Gender
Age
Project
ICIcluster
B cells naive
B cells memory
Plasma cells
T cells CD8
T cells CD4 naive
T cells CD4 memory resting
T cells CD4 memory activated
T cells follicular helper
T cells regulatory (Tregs)
T cells gamma delta
NK cells resting
NK cells activated
Monocytes
Macrophages M0
Macrophages M1
Macrophages M2
Dendritic cells resting
Dendritic cells activated
Mast cells resting
Mast cells activated
Eosinophils
Neutrophils
StromalScore
ImmuneScore
Fustate
Alive
Dead
N
N0
N1~3
T
T1~2
T3~4
Gender
Female
Male
Age
<=65
>65
Project
GSE11969
TCGA
ICIcluster
A
B
C

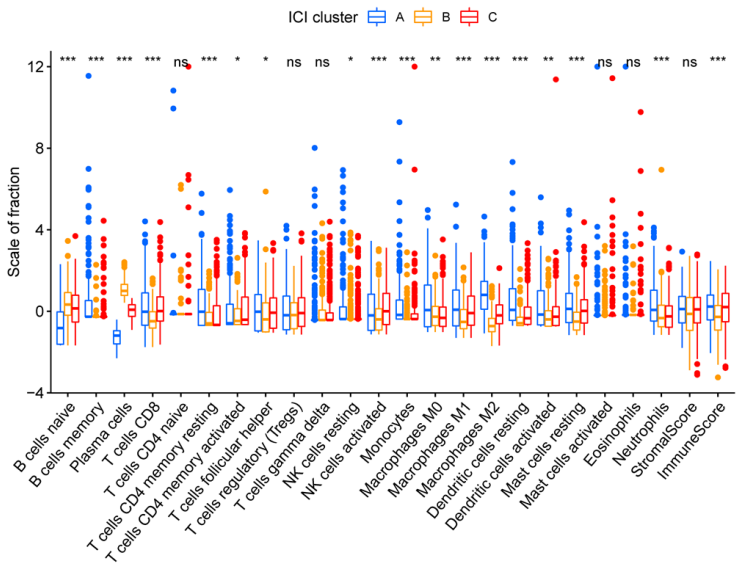
C
ICI cluster A B C
Scale of fraction
12
8
4
0
−4
B cells naive
B cells memory
Plasma cells
T cells CD8
T cells CD4 naive
T cells CD4 memory resting
T cells CD4 memory activated
T cells follicular helper
T cells regulatory (Tregs)
T cells gamma delta
NK cells resting
NK cells activated
Monocytes
Macrophages M0
Macrophages M1
Macrophages M2
Dendritic cells resting
Dendritic cells activated
Mast cells resting
Mast cells activated
Eosinophils
Neutrophils
StromalScore
ImmuneScore

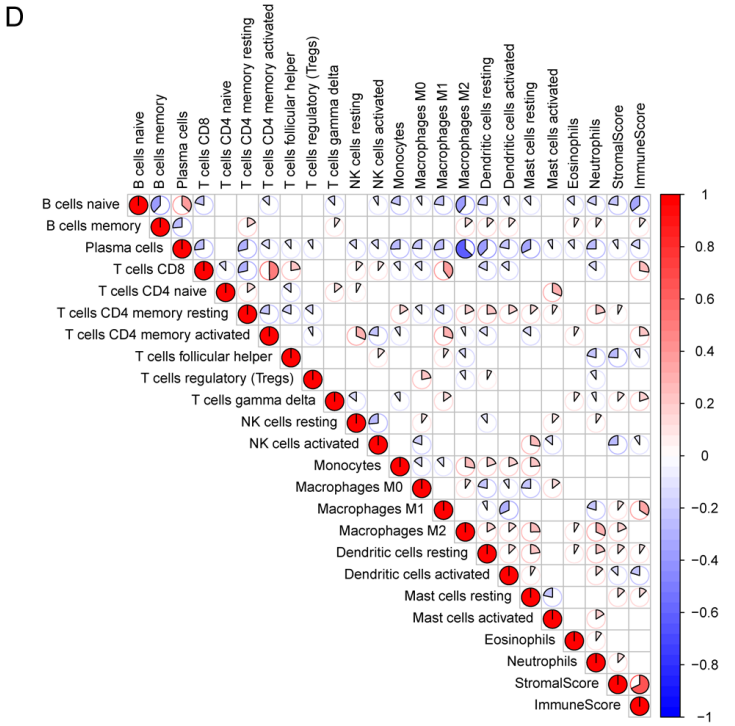
D
B cells naive
B cells memory
Plasma cells
T cells CD8
T cells CD4 naive
T cells CD4 memory resting
T cells CD4 memory activated
T cells follicular helper
T cells regulatory (Tregs)
T cells gamma delta
NK cells resting
NK cells activated
Monocytes
Macrophages M0
Macrophages M1
Macrophages M2
Dendritic cells resting
Dendritic cells activated
Mast cells resting
Mast cells activated
Eosinophils
Neutrophils
StromalScore
ImmuneScore
1
0.8
0.6
0.4
0.2
0
−0.2
−0.4
−0.6
−0.8
−1

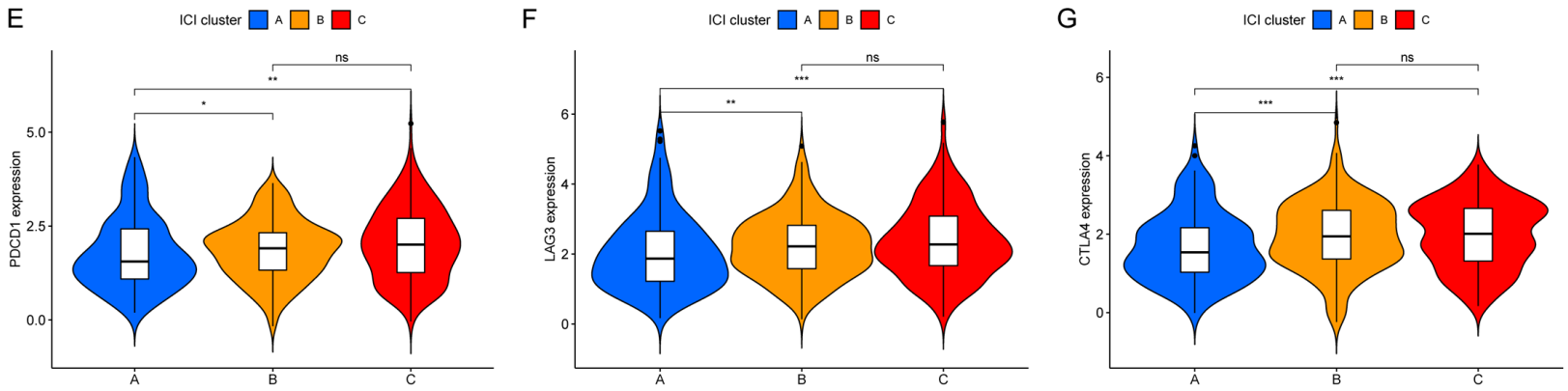

Figure 2. Profile of immune cell infiltration in TMB. (A) The overall survival for different ICI classes shown by Kaplan-Meier plotter (P=0.232). All LUAD-patients were divided into three ICI clusters based on the ICI. (B) The heatmap was made by CIBERSORT algorithm including unsupervised clustering of 22 tumor-infiltrating immune cells in three clusters from 2 LUAD datasets. Fustate, gender, age, and TN stage were included in three clusters. (C) The fraction of tumor-infiltrating immune cells (TIICs) and immune and stromal scores in three clusters were computed by ESTIMATE R package. Results with significant differences were found for immune score. (D) Correlation of intrinsic relativity of 22 TIICs in TMB based on Corrplot R package. Red markers imply positive correlation; blue markers imply inverse correlation. (E-G) Expression difference of PDCD1 (E), LAG3 (F), and CTLA4 (G) in cluster A, B, and C. *P<0.05; **P<0.01; ***P<0.001; ns, not significant; ICI, immune cell infiltration; LUAD, Lung adenocarcinoma; TMB, Tumor mutational burden.

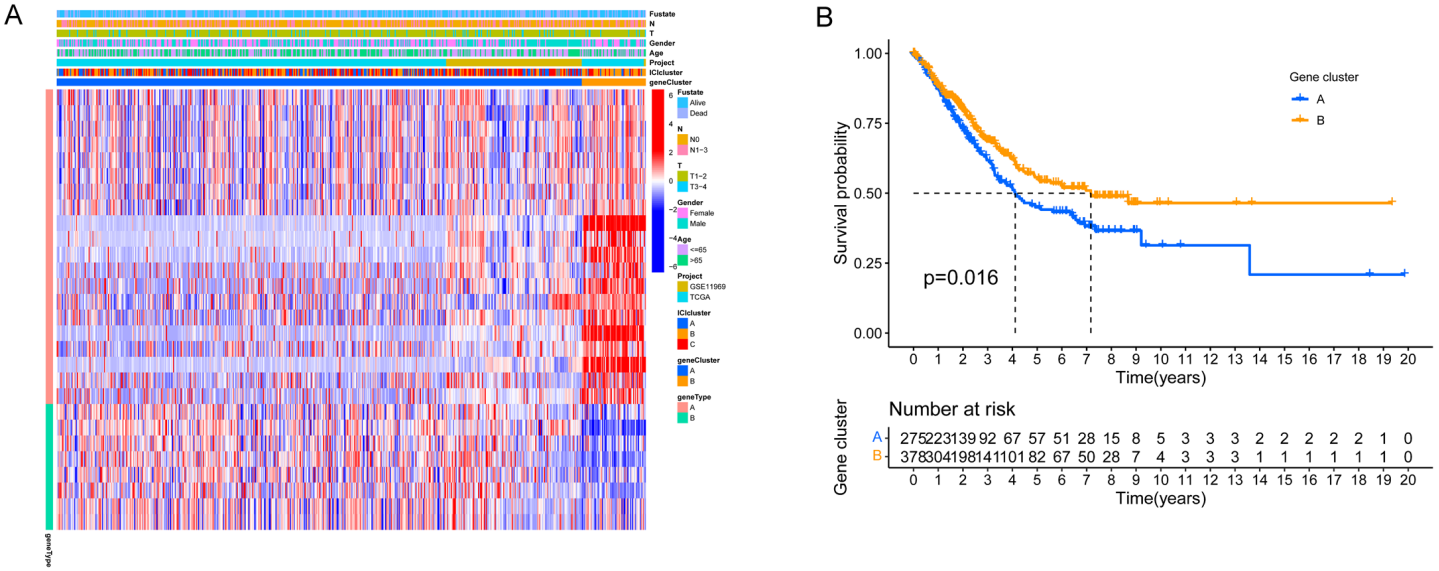

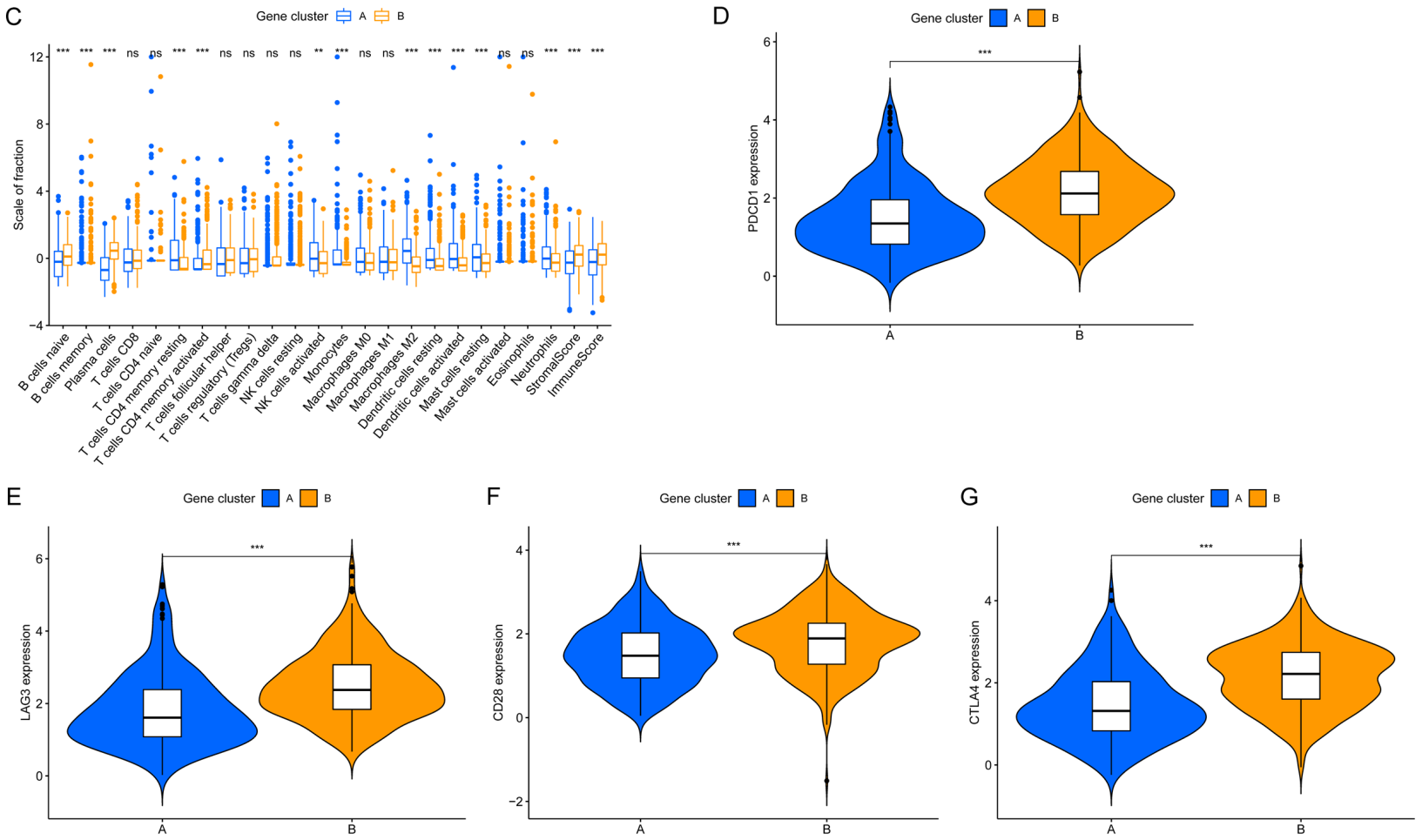

Figure 3. Discrimination of immune gene subtypes. (A) The heatmap shows that gene clusters were classified into two subgroups from differentially expressed genes: gene clusters A and B, based on the analysis of unsupervised clustering. (B) Overall survival compared among three clusters through Kaplan-Meier plotter. (C) Difference comparison of cellular fraction between two gene clusters, including TIICs fraction, immune, and stromal scores. (D-G) Expression of PDCD1 (D), LAG3 (E), CD28 (F), and CTLA4 (G) in clusters A, and B. *P<0.05; **P<0.01; ***P<0.001; ns, not significant.

Immune cell infiltration score model

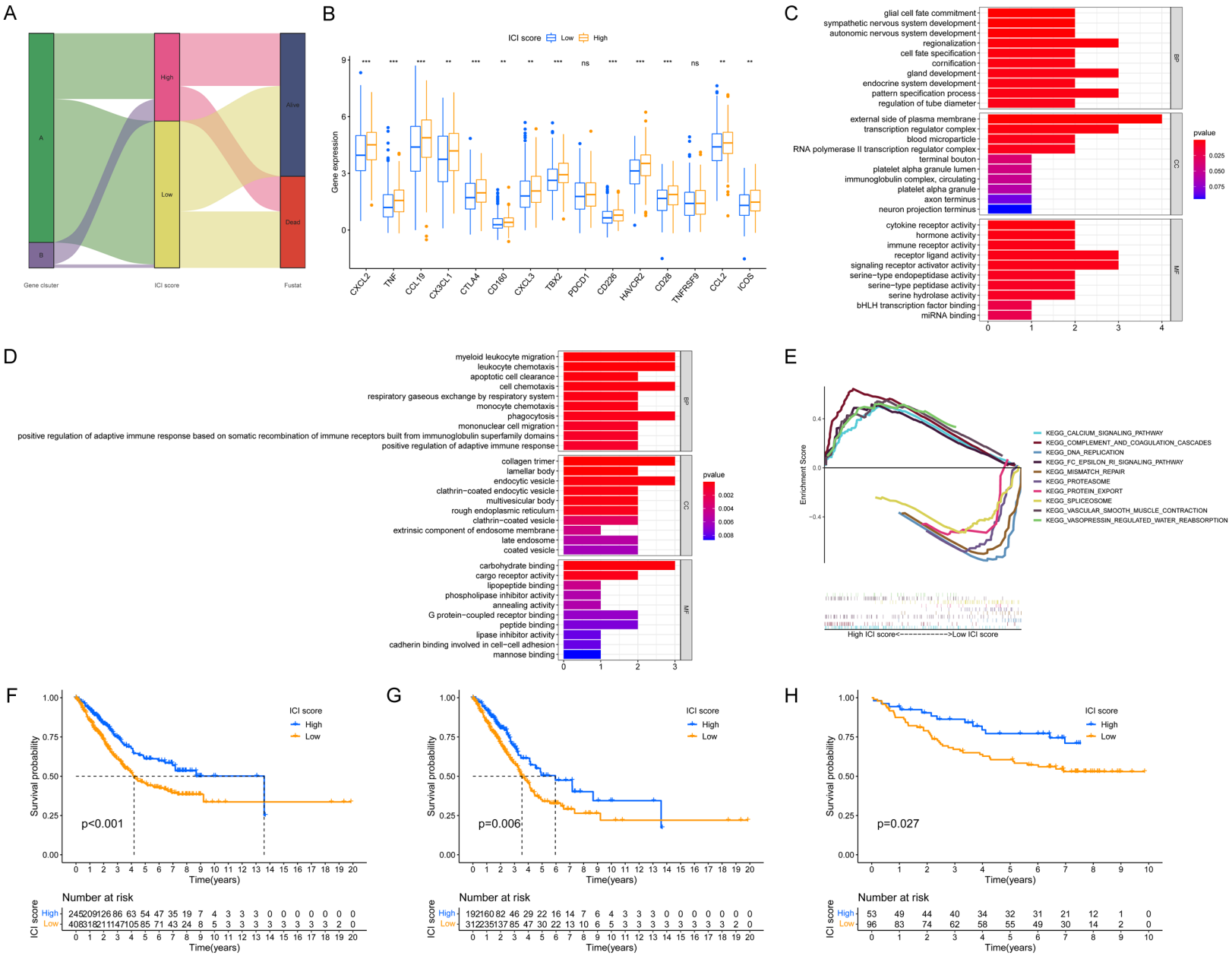

Figure 4. Establishment and analysis of ICI score model. A. The alluvial diagram explained the correlation between gene cluster, ICI score, and patient fustate. B. Expression of immune checkpoint/chemotactic-related gene in two subgroups. C, D. GO enrichment analysis in ICI gene signature A and B. E. GSEA revealed significantly enriched pathways in high/low ICI score groups. F-H. Overall survival in TCGA-LUAD data, GEO data, as well as combined TCGA-LUAD and GEO data. ICI, immune cell infiltration; LUAD, Lung adenocarcinoma.

bined TCGA-LUAD and GEO cohorts (P<0.001), respectively (**Figure 4F-H**).

The correlation between immune cell infiltration score and tumor mutational burden (TMB)

The connection between TMB and ICI can contribute to the prediction of immunotherapy response, and research indicated that patients who receive immune checkpoint therapy tend to have higher TMB [31, 32]. Hence, we explored the relevance between TMB and ICI. The results showed that a low ICI score had a higher level of TMB than a high ICI score had (P<0.001) (**Figure 5A**). Moreover, an inverse correlation was found between TMB and ICI (r=-0.25, P<0.001) (**Figure 5B**). Next, we compared the survival difference of patients between high and low TMB subgroups, and there was no statistical difference (**Figure 5C**). We further discussed the survival differences in the combined group (L-TMB & L-ICI score vs L-TMB & H-ICI score; H-TMB & L-ICI score vs H-TMB & H-ICI score; L: Low, H: High, vs: versus). The H-TMB & H-ICI score group had a worse survival trend (**Figure 5D**). Also, we identified 20 genes with high somatic mutation rates to clarify the cor-relationship between ICI and TMB (**Figure 5E**, **5F**). All results indicated that ICI was a prognostic predictor independent of TMB.

Correlation between ICI score and clinical features of LUAD patients

The correlation between ICI score and clinical features was analyzed to clarify the prognostic value of ICI to LUAD patients, and clinical features including T (T1-2 vs T3-4), N (N0 vs N1-3), and gender (female vs male). Early-stage and male patients with high ICI score have more prolonged survival benefits (N0, P= 0.001; T1-2, P<0.001; male, P=0.001) (**Figure 6A-F**). These results indicated that early-stage and male LUAD patients may be more sensitive to immune checkpoint therapy.

Discussion

Lung adenocarcinoma (LUAD) has high mortality rate among all cancers [33]. Immune checkpoint therapy has provided a new landscape for better clinical survival, but a low immune checkpoint response is a major problem in treatment; one of the important reasons lies in TME-induced immunosuppression [34, 35]. Consequently, we developed an ICI scoring system for TME quantification to facilitate targeted TME for immunotherapy.

In this study, the combined patient samples from the TCGA-LUAD and GSE11969 profiles were divided into three clusters (ICI clusters A, B, and C). Evidence has indicated that the infiltration of CD4-activated memory T cells and activated NK cells were correlated with prolonged survival of patients [36-38]. The two types of ICIs were richer in ICI cluster C than in other clusters. Moreover, the expression level of important immune checkpoint molecules including PDCD1, LAG3, and CTLA4, was higher in ICI cluster C compared to other groups. The above results confirmed that patients in ICI cluster C were highly sensitive to immune checkpoint therapy and may exhibit an ideal effect on immune checkpoint molecules such as CTLA4.

Furthermore, we classified differentially expressed genes into two groups (gene clusters A and B). The higher proportion of naive B cells, activated memory CD4 T cells, and stromal/immune score in the gene cluster B conformed to a better prognosis, which verified the conclusion that a high immune and stromal score have better survival benefits [39-41]. These results further demonstrated the feasibility of ICI score for predicting the prognosis and immunotherapy of LUAD patients.

Based on PCA, patients were dichotomized into high and low ICI score subgroups. All immune checkpoint genes except TNFRSF9 and PDCD1 showed a higher expression in the high ICI score group, which means that high ICI scores provide a more favorable environment for patients to receive immune checkpoint therapy. Next, we screened the top three genes with high somatic mutation rates in high and low ICI score groups, namely TP53, TTN, and MUC16.

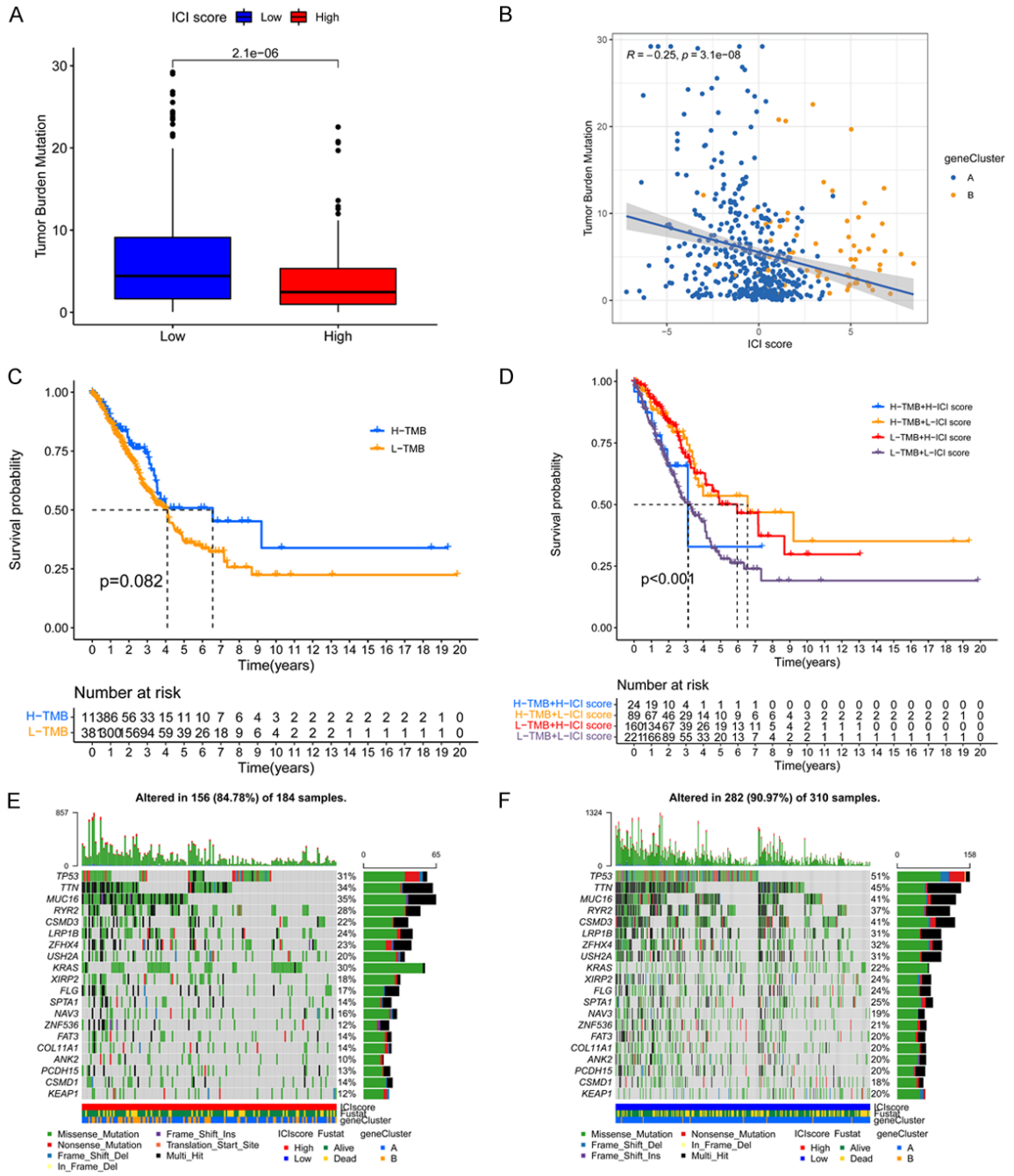

Figure 5. Correlation between immune cell infiltration score and tumor mutational burden. A. Potential relevance between TMB and ICI (P<0.0001). B. Scatterplots proved an inverse correlation between TMB and ICI (r=-0.25, P<0.001). C. Survival difference of patients in high/low TMB subgroups. D. Survival difference of patients in the combined TMB and ICI groups. E, F. The correlatiion between ICI and TMB in high/low ICI groups was based on 20 top genes with the highest somatic mutation frequency. ICI, immune cell infiltration; TMB, Tumor mutational burden.

Research indicated that mutations of TP53, TTN, and MUC16 were associated with TMB [42-44]. TP53 mutation had a higher TMB and was connected to poor prognosis of patients [45]. A high mutation load of TTN and MUC16 represented higher TMB and was positively correlated with patient's prognosis [42, 46]. We conclude that TP53, TTN, and MUC16 may be therapeutic targets for LUAD in the field of immunotherapy.

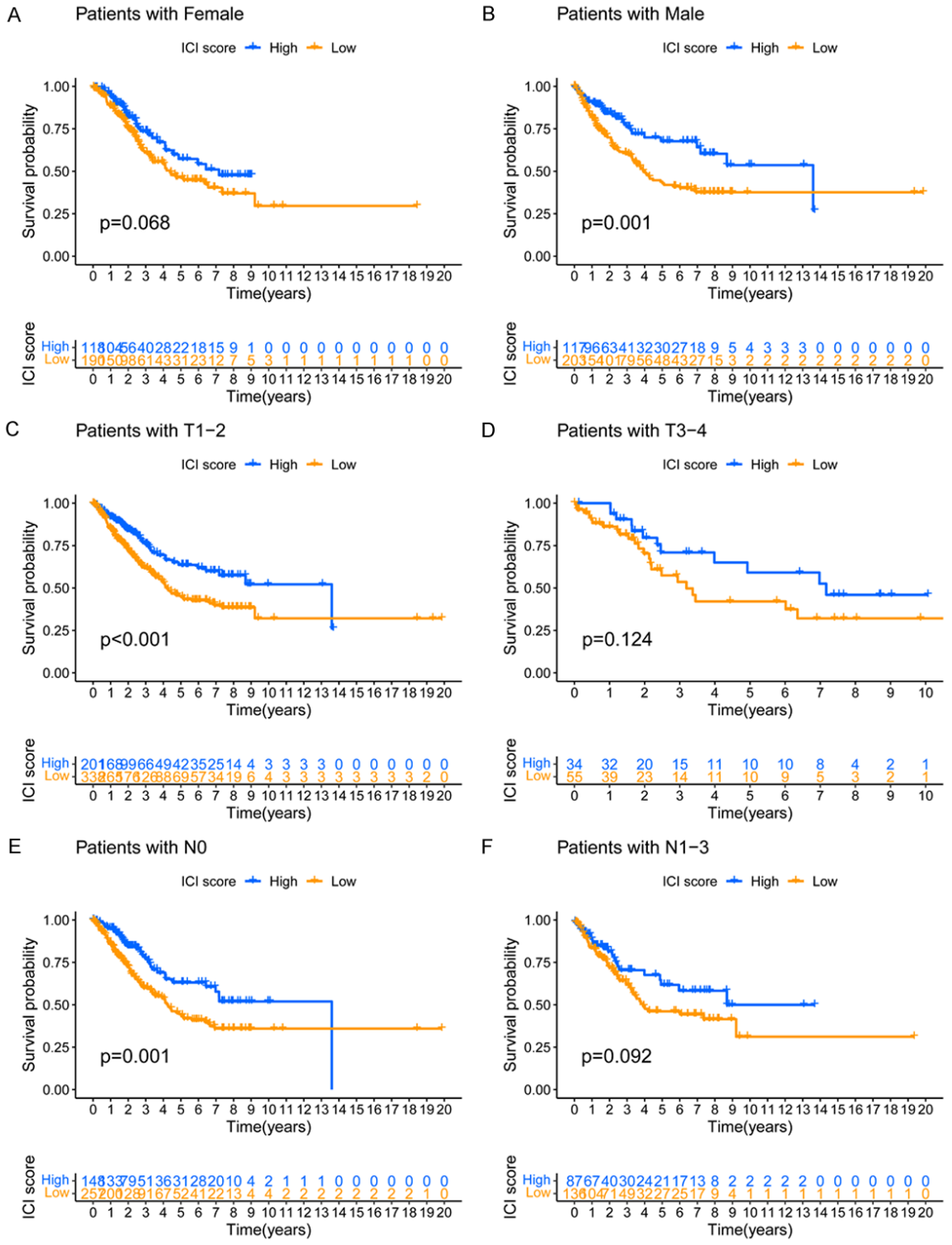

Figure 6. Correlation between ICI score and clinical features of LUAD patients. (A, B) Kaplan-Meier curves for high- and low-ICI scores of females (A) and males (B) in the TCGA-LUAD and GSE11969 cohorts. (C-F) Kaplan-Meier curves for the high- and low-ICI scores of patients with T1-2 (C), patients with T3-4 (D), patients with N0 (E), and patients with N1-3 (F) in the TCGA-LUAD and GSE11969 cohorts. Early-stage and male patients in the low ICI score group had more pronounced survival (N0, P=0.001; T1-2, P<0.001; male, P=0.001). ICI, immune cell infiltration; LUAD, Lung adenocarcinoma.

However, the inverse correlation between TMB and ICI is not consistent with previous conclusions [47]. Thus, the mechanism of interaction between the TMB and ICI needs to be further explored, to see whether other factors are involved.

There are some weaknesses in this study, which need to be further improved. The relationship between ICI and TMB was not further explored. Lack of complete information resulted in some patient data not being strictly filtered. We did only a bioinformatic analysis and lacked the corresponding wet lab experiments to further validate the feasibility of the ICI scoring system.

In this research, we systematically constructed the ICI scoring system based on TME. The feasibility of its application in immune checkpoint therapy for LUAD patients was verified, specifically reflected in screening for sensitive immune checkpoints for patients as a treatment reference. The scoring system can accurately predict the overall survival of LUAD patients, which has value to monitor the disease and evaluate prognosis.

Acknowledgements

We sincerely appreciate TCGA and GEO databases that provided patient information and data. The funding was provided by the Hunan Provincial Health Commission (Nos. 202202-082769), the Science and Technology Program of Changsha city (Nos. KQ1907130), and the research, industrialization and clinical evaluation of KL-6 kit for diagnosis of interstitial pneumonia (Nos. kh2201256).

Disclosure of conflict of interest

None.

Abbreviations

ICI, Immune Cell Infiltration; TME, Tumor Microenvironment; LUAD, Lung Adenocarcinoma; PCA, Principal-component Analysis; NSCLC, Non-small Cell Lung Cancer; TAM, Tumor-associated Macrophages; TPM, Transcripts Per Kilobase Million; TCGA, The Cancer Genome Atlas; GEO, Gene Expression Omnibus; DEGs, Differentially Expressed Genes; PC1, Principal Component 1; GO, Gene Ontology; GSEA, Gene Set Enrichment Analysis; TMB, Tumor Mutational Burden.

Address correspondence to: Drs. Weiguo Qing and Yi Wu, Department of Laboratory, The First Affiliated Hospital of Hunan Normal University, No. 90 Pingchuan Road, Yuelu District, Changsha 410005, Hunan, China. E-mail: 87545387@qq.com (WGQ); wuyi19701210@sina.com (YW)

References

[1] Seguin L, Durandy M and Feral CC. Lung adenocarcinoma tumor origin: a guide for personalized medicine. Cancers (Basel) 2022; 14: 1759.
[2] Shiba-Ishii A. Significance of stratifin in early progression of lung adenocarcinoma and its potential therapeutic relevance. Pathol Int 2021; 71: 655-665.
[3] Zhang H, Guo L and Chen J. Rationale for lung adenocarcinoma prevention and drug development based on molecular biology during carcinogenesis. Onco Targets Ther 2020; 13: 3085-3091.
[4] Succony L, Rassl DM, Barker AP, McCaughan FM and Rintoul RC. Adenocarcinoma spectrum lesions of the lung: detection, pathology and treatment strategies. Cancer Treat Rev 2021; 99: 102237.
[5] Sadeghi Rad H, Monkman J, Warkiani ME, Ladwa R, O'Byrne K, Rezaei N and Kulasinghe A. Understanding the tumor microenvironment for effective immunotherapy. Med Res Rev 2021; 41: 1474-1498.
[6] Genova C, Dellepiane C, Carrega P, Sommariva S, Ferlazzo G, Pronzato P, Gangemi R, Filaci G, Coco S and Croce M. Therapeutic implications of tumor microenvironment in lung cancer: focus on immune checkpoint blockade. Front Immunol 2021; 12: 799455.
[7] Anderson NM and Simon MC. The tumor microenvironment. Curr Biol 2020; 30: R921-R925.
[8] Altorki NK, Markowitz GJ, Gao D, Port JL, Saxena A, Stiles B, McGraw T and Mittal V. The lung microenvironment: an important regulator of tumour growth and metastasis. Nat Rev Cancer 2019; 19: 9-31.
[9] Ho T and Msallam R. Tissues and tumor microenvironment (TME) in 3D: models to shed light on immunosuppression in cancer. Cells 2021; 10: 831.
[10] Sadeghirad H, Bahrami T, Layeghi SM, Yousefi H, Rezaei M, Hosseini-Fard SR, Radfar P, Warkiani ME, O'Byrne K and Kulasinghe A. Immunotherapeutic targets in non-small cell lung cancer. Immunology 2023; 168: 256-272.
[11] Li T and Qiao T. Unraveling tumor microenvironment of small-cell lung cancer: implications for immunotherapy. Semin Cancer Biol 2022; 86: 117-125.
[12] Li T and Qiao T. Unraveling tumor microenvironment of small-cell lung cancer: implications for

immunotherapy. Semin Cancer Biol 2022; 86: 117-125.
[13] Joyce JA. Therapeutic targeting of the tumor microenvironment. Cancer Cell 2005; 7: 513-520.
[14] Osipov A, Saung MT, Zheng L and Murphy AG. Small molecule immunomodulation: the tumor microenvironment and overcoming immune escape. J Immunother Cancer 2019; 7: 224.
[15] Jahchan N, Binnewies M, Pollack J, Mehta R, Dash S, Tun C, Lu E, Du X, Baker K, Reyno L and Sriram V. Abstract LB071: tuning the tumor myeloid microenvironment (TME) by targeting TREM2+ tumor-associated macrophages to overcome resistance to immune checkpoint inhibitors. 2021.
[16] Liu Y, Zhou X and Wang X. Targeting the tumor microenvironment in B-cell lymphoma: challenges and opportunities. J Hematol Oncol 2021; 14: 125.
[17] Zeng Y, Zeng Y, Yin H, Chen F, Wang Q, Yu X and Zhou Y. Exploration of the immune cell infiltration-related gene signature in the prognosis of melanoma. Aging (Albany NY) 2021; 13: 3459-3482.
[18] Zuo S, Wei M, Wang S, Dong J and Wei J. Pan-cancer analysis of immune cell infiltration identifies a prognostic immune-cell characteristic score (ICCS) in lung adenocarcinoma. Front Immunol 2020; 11: 1218.
[19] Smit MJ, Schlecht-Louf G, Neves M, van den Bor J, Penela P, Siderius M, Bachelerie F and Mayor F Jr. The CXCL12/CXCR4/ACKR3 axis in the tumor microenvironment: signaling, crosstalk, and therapeutic targeting. Annu Rev Pharmacol Toxicol 2021; 61: 541-563.
[20] Rutland JW, Gill CM, Loewenstern J, Arib H, Pain M, Umphlett M, Kinoshita Y, McBride RB, Bederson J, Donovan M, Sebra R, Shrivastava RK and Fowkes M. NF2 mutation status and tumor mutational burden correlate with immune cell infiltration in meningiomas. Cancer Immunol Immunother 2021; 70: 169-176.
[21] Thota R, Christensen B, Fulde G, Lewis MA, Haslem DS, Rhodes TD, Nadauld L and Barker T. Characterization of the tumor mutation burden in hepatobiliary tumors. J Clin Oncol 2019; 37.
[22] Xu Q, Chen S, Hu Y and Huang W. Landscape of immune microenvironment under immune cell infiltration pattern in breast cancer. Front Immunol 2021; 12: 711433.
[23] Jiang T, Shi J, Dong Z, Hou L, Zhao C, Li X, Mao B, Zhu W, Guo X, Zhang H, He J, Chen X, Su C, Ren S, Wu C and Zhou C. Genomic landscape and its correlations with tumor mutational burden, PD-L1 expression, and immune cells infiltration in Chinese lung squamous cell carcinoma. J Hematol Oncol 2019; 12: 75.
[24] Degenhardt F, Seifert S and Szymczak S. Evaluation of variable selection methods for random forests and omics data sets. Brief Bioinform 2019; 20: 492-503.
[25] Migenda N, Moller R and Schenck W. Adaptive dimensionality reduction for neural network-based online principal component analysis. PLoS One 2021; 16: e0248896.
[26] Tang X, Liu M, Luo X, Zhu M, Huang S and Pan X. The prognostic value of a tumor microenvironment-based immune cell infiltration score model in colon cancer. Front Oncol 2021; 11: 728842.
[27] Dutta S and Datta S. A rank-sum test for clustered data when the number of subjects in a group within a cluster is informative. Biometrics 2016; 72: 432-440.
[28] Liu Y and Chen W. A SAS macro for testing differences among three or more independent groups using Kruskal-Wallis and Nemenyi tests. J Huazhong Univ Sci Technolog Med Sci 2012; 32: 130-134.
[29] Liu J, Wang Y, Yuan S, Wei J and Bai J. Construction of an immune cell infiltration score to evaluate the prognosis and therapeutic efficacy of ovarian cancer patients. Front Immunol 2021; 12: 751594.
[30] Zhao Y, Guo Y, Xiao Y, Zhu R, Sun W, Huang W, Liang D, Tang L, Zhang F, Zhu D and Wu JL. The effects of online homeschooling on children, parents, and teachers of grades 1-9 during the COVID-19 pandemic. Med Sci Monit 2020; 26: e925591.
[31] Wen F, Ruan S, Huang W, Chen X, Wang Y, Gu S, Liu J, Liu S and Shu P. Prognostic value of tumor mutational burden related to immune infiltration in cervical squamous cell carcinoma. Front Med (Lausanne) 2021; 8: 755657.
[32] Yuan C, Xiang L, Cao K, Zhang J, Luo Y, Sun W, Zhang N, Ren J, Zhang J, Gong Y and Xie C. The prognostic value of tumor mutational burden and immune cell infiltration in esophageal cancer patients with or without radiotherapy. Aging (Albany NY) 2020; 12: 4603-4616.
[33] Jiang J, Jin Z, Zhang Y, Peng L, Zhang Y, Zhu Z, Wang Y, Tong, Yang Y, Wang J, Yang Y and Xiao K. Robust prediction of immune checkpoint inhibition therapy for non-small cell lung cancer. Front Immunol 2021; 12: 646874.
[34] Wei SC, Duffy CR and Allison JP. Fundamental mechanisms of immune checkpoint blockade therapy. Cancer Discov 2018; 8: 1069-1086.
[35] Wei G, Zhang H, Zhao H, Wang J, Wu N, Li L, Wu J and Zhang D. Emerging immune checkpoints in the tumor microenvironment: implications for cancer immunotherapy. Cancer Lett 2021; 511: 68-76.
[36] Xu JY, Zhang C, Wang X, Zhai L, Ma Y, Mao Y, Qian K, Sun C, Liu Z, Jiang S, Wang M, Feng L,

Zhao L, Liu P, Wang B, Zhao X, Xie H, Yang X, Zhao L, Chang Y, Jia J, Wang X, Zhang Y, Wang Y, Yang Y, Wu Z, Yang L, Liu B, Zhao T, Ren S, Sun A, Zhao Y, Ying W, Wang F, Wang G, Zhang Y, Cheng S, Qin J, Qian X, Wang Y, Li J, He F, Xiao T and Tan M. Integrative proteomic characterization of human lung adenocarcinoma. Cell 2020; 182: 245-261, e17.

[37] Wang L, Wei Q, Zhang M, Chen L, Li Z, Zhou C, He M, Wei M and Zhao L. Identification of the prognostic value of immune gene signature and infiltrating immune cells for esophageal cancer patients. Int Immunopharmacol 2020; 87: 106795.

[38] Uthaman S, Cutshaw G, Ghazvini S and Bardhan R. Nanomaterials for natural killer cell-based immunoimaging and immunotherapies in cancer. ACS Appl Mater Interfaces 2022; [Epub ahead of print].

[39] Lin J, Wu C, Ma D and Hu Q. Identification of P2RY13 as an immune-related prognostic biomarker in lung adenocarcinoma: a public database-based retrospective study. PeerJ 2021; 9: e11319.

[40] Ma Q, Chen Y, Xiao F, Hao Y, Song Z, Zhang J, Okuda K, Um SW, Silva M, Shimada Y, Si C and Liang C. A signature of estimate-stromal-immune score-based genes associated with the prognosis of lung adenocarcinoma. Transl Lung Cancer Res 2021; 10: 1484-1500.

[41] Qi X, Qi C, Qin B, Kang X, Hu Y and Han W. Immune-stromal score signature: novel prognostic tool of the tumor microenvironment in lung adenocarcinoma. Front Oncol 2020; 10: 541330.

[42] Yang Y, Zhang J, Chen Y, Xu R, Zhao Q and Guo W. MUC4, MUC16, and TTN genes mutation correlated with prognosis, and predicted tumor mutation burden and immunotherapy efficacy in gastric cancer and pan-cancer. Clin Transl Med 2020; 10: e155.

[43] Xie X, Tang Y, Sheng J, Shu P, Zhu X, Cai X, Zhao C, Wang L and Huang X. Titin mutation is associated with tumor mutation burden and promotes antitumor immunity in lung squamous cell carcinoma. Front Cell Dev Biol 2021; 9: 761758.

[44] Li X, Zhang X, Niu Y and Ma T. Investigating the various predictive values of TP53 mutations for response to immune checkpoint inhibitors (ICIs) in different solid tumors. J Clin Oncol 2022; 40: e14581.

[45] Wen XM, Xu ZJ, Jin Y, Xia PH, Ma JC, Qian W, Lin J and Qian J. Association analyses of TP53 mutation with prognosis, tumor mutational burden, and immunological features in acute myeloid leukemia. Front Immunol 2021; 12: 717527.

[46] Oh JH, Jang SJ, Kim J, Sohn I, Lee JY, Cho EJ, Chun SM and Sung CO. Spontaneous mutations in the single TTN gene represent high tumor mutation burden. NPJ Genom Med 2020; 5: 33.

[47] Ma T, Jiao J, Huo R, Li X, Fang G, Zhao Q, Liu W, Han X, Xi C, Wang Y and Shang Y. PD-L1 expression, tumor mutational burden, and immune cell infiltration in non-small cell lung cancer patients with epithelial growth factor receptor mutations. Front Oncol 2022; 12: 922899.

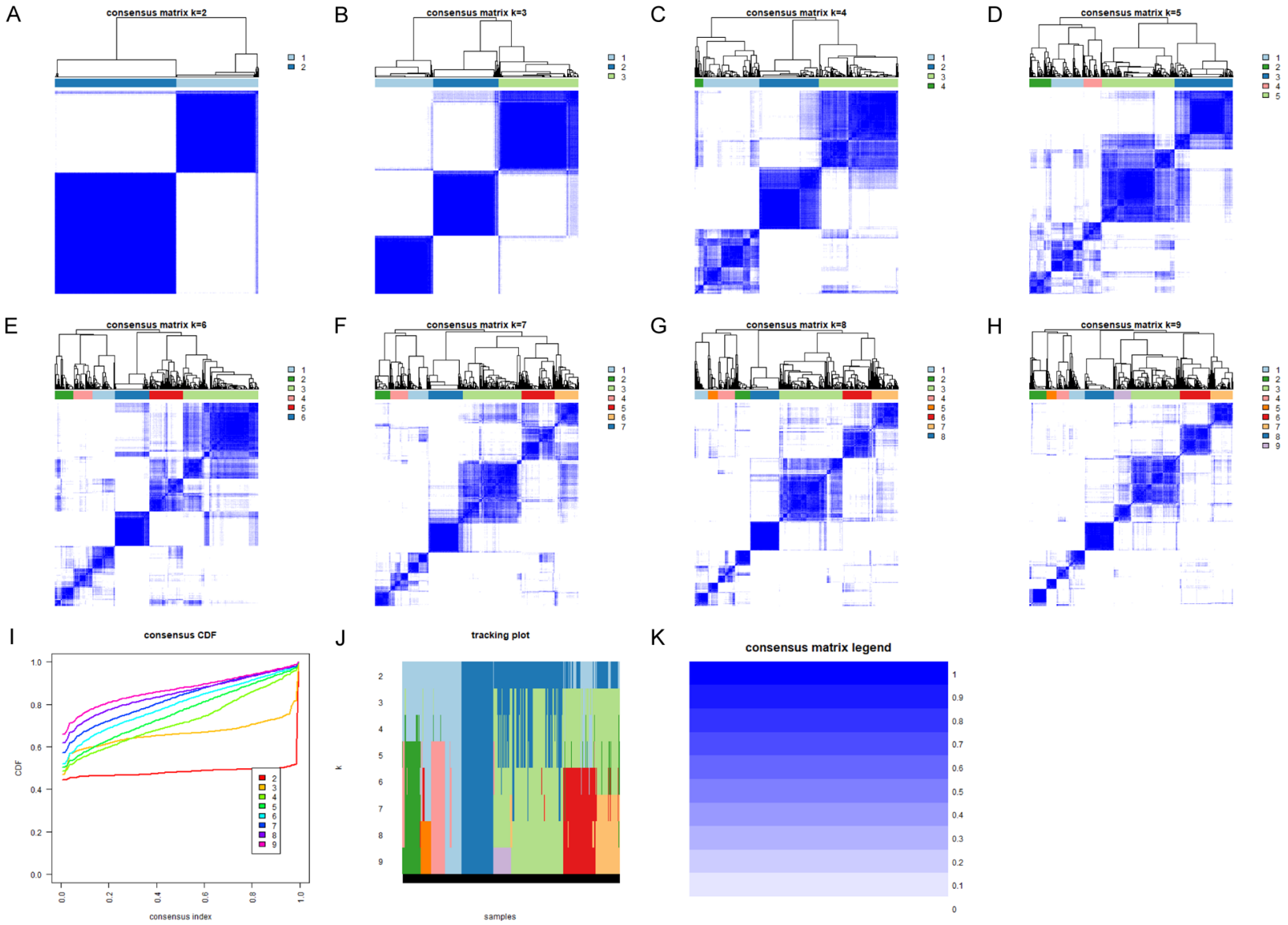

Supplementary Figure 1. A-K. Optimal number of three clusters (ICI cluster A, B, and C) based on k=3 was discerned. ICI, immune cell infiltration.

Supplementary Table 1. Differentially expressed genes between clusters A and B

id	logFC	AveExpr	t	*P*.value
IGHM	2.981221825	6.901363296	23.44468359	1.33E-88
IGKC	2.066105056	8.679533219	15.60817719	6.85E-47
IGLC2	1.722365973	8.052165139	13.32024741	5.67E-36
CD79A	1.569415655	4.084141125	12.84012896	8.44E-34
DERL3	1.161818773	3.651334884	12.35003362	1.25E-31
IGHG1	1.854251951	8.517641733	11.63744194	1.43E-28
TNFRSF17	1.059713137	2.316771765	9.805619191	2.89E-21
MRC1	-1.1492739	3.919369826	-8.970522126	3.11E-18
IGHG4	1.53162762	6.916980503	8.545058811	9.10E-17
ANXA1	-1.007774134	5.57963067	-8.16748329	1.64E-15
ASCL1	1.661396968	0.977465115	7.675837552	6.03E-14
CCL13	-1.073956351	3.796867086	-7.452823902	2.92E-13
SST	1.363431808	0.598443991	7.37154725	5.14E-13
MMP28	-1.186203609	2.951306076	-7.209077881	1.57E-12
MARCO	-1.110053682	4.323382599	-6.809309485	2.23E-11
KLK14	1.057828715	1.116113102	6.721151671	3.94E-11
CD1A	-1.001584202	2.118293984	-6.288787217	5.87E-10
HOXB9	1.061110197	1.21633933	6.272326064	6.48E-10
BARX1	1.299713319	1.822751219	6.058165362	2.33E-09
SOX2	1.066246069	2.557107026	5.811383143	9.70E-09
GFRA3	1.03834627	2.468549802	5.508891143	5.20E-08
KLK12	1.058740174	1.426886303	4.818419555	1.80E-06
MSMB	1.287439816	3.348585668	4.589965692	5.32E-06
CALCA	1.223007096	1.359008937	4.438024525	1.07E-05
CRLF1	1.022896324	3.521698288	4.423678715	1.14E-05
SFTPA1	-1.240762065	7.221048167	-4.332764345	1.71E-05
FGB	1.086825495	2.253820694	3.79330134	0.000162496
SFTPA2	-1.061676487	7.475976141	-3.745362898	0.00019609

Supplementary Table 2. Differentially expressed genes between clusters A and C

id	logFC	AveExpr	t	*P*.value
IGHM	1.947113466	6.901363296	16.00251112	7.44E-49
IGKC	1.490925083	8.679533219	11.77070298	3.91E-29
CD79A	1.091776385	4.084141125	9.334947837	1.57E-19
IGLC2	1.086364453	8.052165139	8.780296757	1.43E-17
IGHG1	1.321415569	8.517641733	8.667123709	3.50E-17
IGHG4	1.043907755	6.916980503	6.086544256	1.97E-09

Supplementary Table 3. Differentially expressed genes between cluster B and C

id	logFC	AveExpr	t	*P*.value
IGHM	-1.034108359	6.901363296	-8.794968287	1.27E-17
ASCL1	-1.173552092	0.977465115	-5.863715337	7.20E-09
CALCA	-1.270896356	1.359008937	-4.987569964	7.85E-07

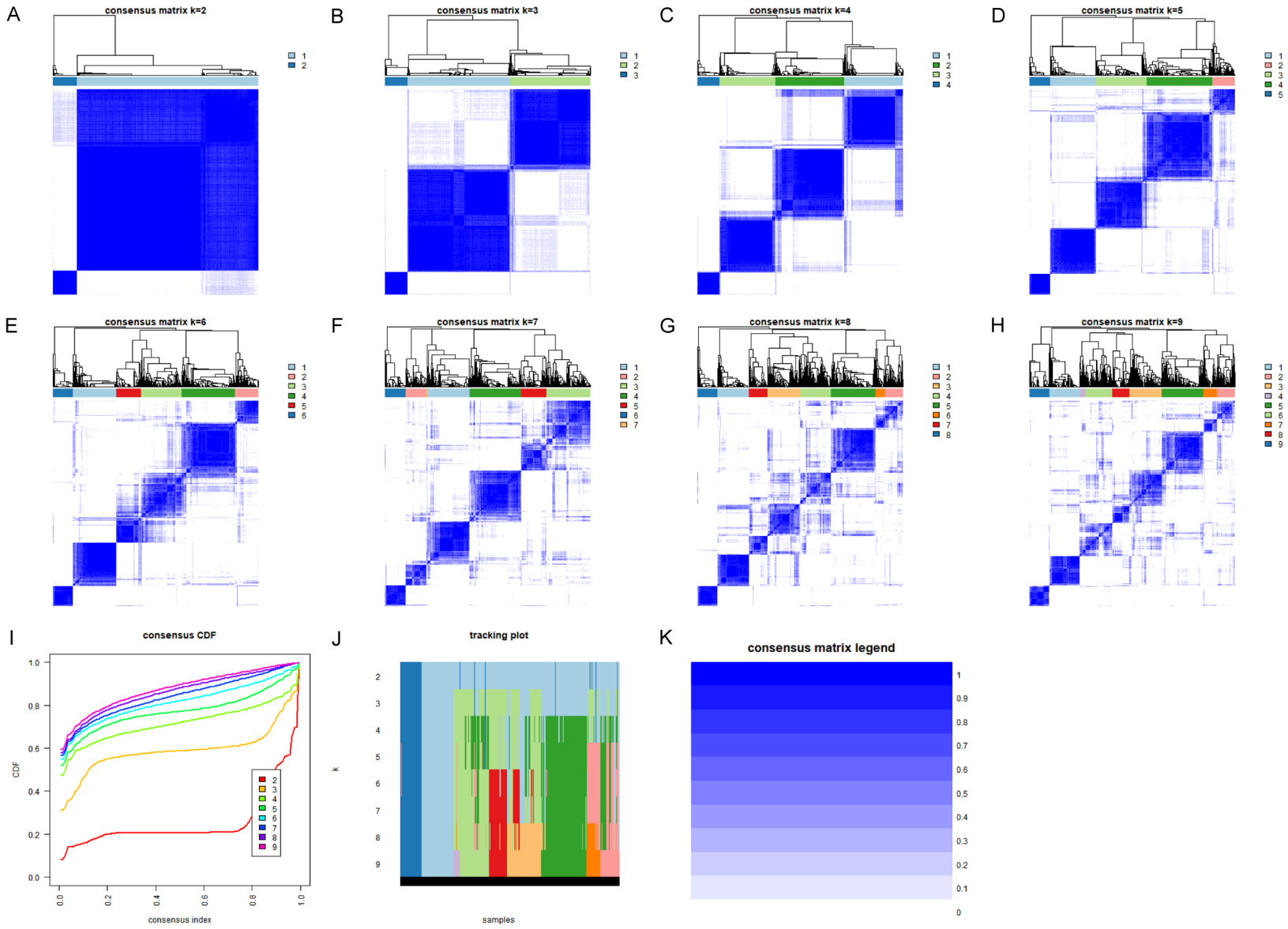

Supplementary Figure 2. A-K. Optimal number of two gene clusters (gene clusters A and B) based on k=2 was discerned.